Check for updates

A tRNA-Acetylating Toxin and Detoxifying Enzyme in *Mycobacterium tuberculosis*

Francesca G. Tomasi,[a] Alexander M. J. Hall,[b] Jessica T. P. Schweber,[a] Charles L. Dulberger,[a] Kerry McGowen,[a] Qingyun Liu,[a] Sarah M. Fortune,[a] Sophie Helaine,[b] Eric J. Rubin[a]

[a]Department of Immunology and Infectious Diseases, Harvard T. H. Chan School of Public Health, Boston, Massachusetts, USA
[b]Department of Microbiology, Harvard Medical School, Boston, Massachusetts, USA

ABSTRACT Toxin-antitoxin (TA) systems allow bacteria to adapt to changing environments without altering gene expression. Despite being overrepresented in *Mycobacterium tuberculosis*, their physiological roles remain elusive. We describe a TA system in *M. tuberculosis* which we named TacAT due to its homology to previously discovered systems in *Salmonella*. The toxin, TacT, blocks growth by acetylating glycyl-tRNAs and inhibiting translation. Its effects are reversed by the enzyme peptidyl tRNA hydrolase (Pth), which also cleaves peptidyl tRNAs that are prematurely released from stalled ribosomes. Pth is essential in most bacteria and thereby has been proposed as a promising drug target for complex pathogens like *M. tuberculosis*. Transposon sequencing data suggest that the *tacAT* operon is nonessential for *M. tuberculosis* growth *in vitro*, and premature stop mutations in this TA system present in some clinical isolates suggest that it is also dispensable *in vivo*. We assessed whether TacT modulates *pth* essentiality in *M. tuberculosis* because drugs targeting Pth might prompt resistance if TacAT is disrupted. We show that *pth* essentiality is unaffected by the absence of *tacAT*. These results highlight a fundamental aspect of mycobacterial biology and indicate that Pth's essential role hinges on its peptidyl-tRNA hydrolase activity. Our work underscores Pth's potential as a viable target for new antibiotics.

IMPORTANCE The global rise in antibiotic-resistant tuberculosis has prompted an urgent search for new drugs. Toxin-antitoxin (TA) systems allow bacteria to adapt rapidly to environmental changes, and *Mycobacterium tuberculosis* encodes more TA systems than any known pathogen. We have characterized a new TA system in *M. tuberculosis*: the toxin, TacT, acetylates charged tRNA to block protein synthesis. TacT's effects are reversed by the essential bacterial enzyme peptidyl tRNA hydrolase (Pth), which is currently being explored as an antibiotic target. Pth also cleaves peptidyl tRNAs that are prematurely released from stalled ribosomes. We assessed whether TacT modulates *pth* essentiality in *M. tuberculosis* because drugs targeting Pth might prompt resistance if TacT is disrupted. We show that *pth* essentiality is unaffected by the absence of this TA system, indicating that Pth's essential role hinges on its peptidyl-tRNA hydrolase activity. Our work underscores Pth's potential as a viable target for new antibiotics.

KEYWORDS *Mycobacterium tuberculosis*, antibiotic resistance, tRNA modification, toxin/antitoxin systems, translation

Mycobacterium tuberculosis, which causes tuberculosis (TB), is a leading cause of global infectious disease mortality (1). The ability of *M. tuberculosis* to regulate its growth in different stressful conditions *in vitro* is thought to be an important part of its success *in vivo*. One of this pathogen's tools for growth regulation is an expansive network of toxin-antitoxin (TA) systems, with at least 100 putative modules that encompass nearly 4%

of *M. tuberculosis*'s coding capacity (2, 3). Most of these systems in *M. tuberculosis* can be grouped into five main families based on sequence homology: VapBC, MazEF, RelBE, HigBA, and ParDE (4, 5). Toxins of TAs are characterized by their general intracellular targets and mechanisms of activity with most known *M. tuberculosis* toxins being RNases that cleave rRNA, mRNA, or tRNA.

In type II TA systems, the most widespread and heavily studied type, a protein antitoxin is bound tightly to its cognate protein toxin and acts to neutralize it (6). If the antitoxin is degraded, the toxin assumes its active form and blocks an essential process such as DNA replication or protein synthesis until antitoxin production resumes (6). Despite being widespread in bacteria, the physiological roles of TA systems are just emerging, with some having been linked to plasmid maintenance, bacteriophage immunity, and the formation of dormant, antibiotic-tolerant persisters (7, 8). TA systems might play a role in *M. tuberculosis*'s ability to withstand host and antibiotic pressures by controlling growth under different stress conditions (4, 9, 10). However, it remains to be determined whether or to what extent they play a role in pathogenesis. A significant barrier to understanding TA systems is the challenge of directly measuring native toxin activity in cells and, therefore, understanding when they are active and how they interact with other enzymes. Because of the nature of TA system autoregulation and posttranslational control, transcription upregulation data alone do not necessarily indicate toxin activation (11). So far, studies investigating TA systems in bacteria often measure activity in cells using ectopic overexpression constructs (4, 5, 12). These studies offer fascinating mechanistic insights but do so in isolation from other intracellular systems, and it has been difficult to link the molecular mechanisms of TA systems to their biological roles.

Recently, a new class of TA systems called TacAT was discovered in *Salmonella* and homologs have since been identified in other species, including *Escherichia coli* and *Klebsiella pneumoniae* (13–17). The toxins in this family are GCN5-related N-acetyltransferases (GNAT) that acetylate aminoacyl tRNA and block the incorporation of an amino acid into a growing peptide chain. TacT's unique mechanism of action – which can be detected using liquid chromatography-coupled mass spectrometry (LCMS) – makes it an appealing TA system to study in the context of bacterial physiology (13, 14, 18, 19). An unusual aspect of TacAT systems is that, while the antitoxin can block toxin activity as seen with other TA systems, the effect can also be reversed via the ubiquitous and essential bacterial enzyme peptidyl tRNA hydrolase (Pth) (13, 14). This enzyme cleaves acetylated amino acids from tRNA molecules, effectively unblocking protein synthesis. TacT's mechanistic connection to an essential enzyme makes it an appealing TA system to study in the context of gene essentiality.

Here, we describe an *M. tuberculosis* homolog of the TacAT TA system, the first of its kind to be identified in this organism. We show that this TA system is encoded by the Rv0918-0919 operon and confirm that Rv0919 encodes a tRNA-acetylating toxin whose activity can be reversed by *M. tuberculosis* Pth (Rv1014c). While *pth* is required for growth in *M. tuberculosis*, transposon sequencing data suggest that the *M. tuberculosis* TacAT operon is dispensable for growth *in vitro*, and we have identified premature stop mutations in this TA system in clinical isolates (20). If TacT activity modulates *pth* essentiality in *M. tuberculosis*, then drugs targeting Pth might prompt resistance if TacAT activity is disrupted as has already happened in clinical isolates. However, we found that while the *tacAT* operon is indeed dispensable, *pth* essentiality is unaffected by the absence of this TA system. Our results indicate that Pth's essential role in *M. tuberculosis* hinges on its function in cleaving peptidyl-tRNA and not acetylated aminoacyl tRNA. Our work underscores Pth's potential as a viable target for new antibiotics, while also highlighting multiple angles from which to study TA systems in *M. tuberculosis*.

RESULTS

Rv0918-0919 encodes a toxin-antitoxin system that inhibits growth by acetylating glycyl-tRNAs. Previous studies have identified over 100 putative TA systems in *M. tuberculosis*, based on genetic architecture and homology to known TA systems (5). The *M. tuberculosis* operon Rv0918-0919 has been computationally flagged as a possible TA system due to its polycistronic organization and the presence of a conserved, DNA-binding ribbon-helix-helix
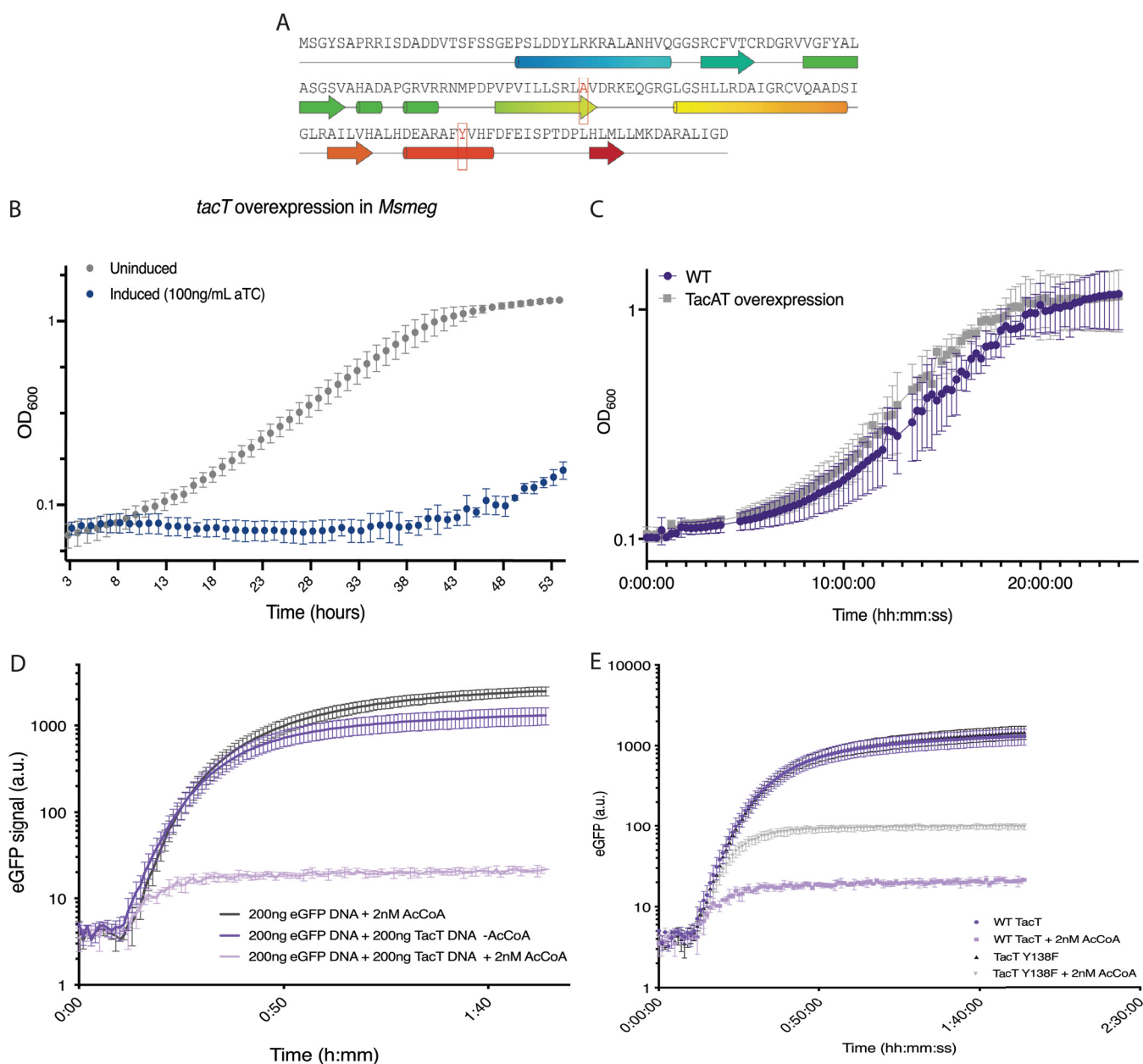
FIG 1 TacT is a toxin that inhibits protein synthesis. (A) Amino acid sequence and high-confidence model of *M. tuberculosis* TacT (Rv0919) generated using the PHYRE2 protein fold recognition server (46), with the final output modeled on the structure of TacT1 from *Salmonella* Typhimurium (PDB: 5fvj) (14). Active site residues in red were mutated for catalytically inactive TacT for subsequent experiments. (B) Exogenous overexpression of TacT (Rv0919) blocks the growth of *Mycobacterium smegmatis* (*Msmeg*). The *M. tuberculosis tacT* gene was cloned under a tetracycline-inducible promoter and integrated into the *M. smegmatis* genome. The addition of anhydrous tetracycline (aTC; 100 ng/mL) leads to overexpression of *tacT*. Strains were diluted to an OD of 0.003 and growth was measured by optical density at 600 nm (OD_{600}). Results are shown from 3 biological replicates. (C) Exogenous expression of *M. tuberculosis* TacAT (Rv0918-0919) does not block the growth of *Mycobacterium smegmatis*. The *M. tuberculosis tacAT* operon was cloned under a constitutive overexpression promoter and integrated into the *M. smegmatis* genome. Strains were diluted to an OD of 0.05 and growth was measured by optical density at 600 nm (OD_{600}). Results are from three replicates. (D) *M. tuberculosis* TacT blocks translation in the presence of acetyl coenzyme A. A TacT expression construct was added to the PURExpress *in vitro* Protein Synthesis kit along with an eGFP expression construct. Protein synthesis was read out as eGFP synthesis and monitored spectrophotometrically at excitation of 488 nm and emission of 509 nm. Results are from technical duplicates. (E) The active site mutation Y138F based on studies in *Salmonella* reduces *M. tuberculosis* TacT toxicity. Cell-free protein synthesis reactions were carried out as in (D). Inactive TacT was made using an Rv0919 expression construct containing the active side residue mutation Y138F. Results are from technical duplicates.

(RHH) domain in the putative antitoxin gene, Rv0918 (Fig. 1A) (5, 21). Rv0919 contains a conserved GNAT domain, and protein BLAST results show >50% sequence identity to the N-acetyltransferase TacAT toxins in *Salmonella* (Fig. 1A) (22).

We hypothesized that Rv0919 encodes a TacT-like toxin that inhibits growth by blocking translation. The closely related but faster-growing, nonpathogenic model organism

Mycobacterium smegmatis (*Msmeg*) does not encode any putative TacAT-like systems (21, 22). Therefore, to study *M. tuberculosis* TacT in isolation from other potential interacting genes, we built an integrating vector carrying Rv0919 under the control of an anhydrous tetracycline (aTC)-inducible promoter. Induced overexpression of Rv0919 in *M. smegmatis* inhibited growth (Fig. 1B), while constitutive expression of the entire Rv0918-0919 operon did not (Fig. 1C), showing that Rv0919 encodes a growth-inhibiting enzyme that is not active in the presence of Rv0918.

We next assessed Rv0919 activity *in vitro* using a cell-free protein synthesis kit. We found that, while GFP could be efficiently expressed in this system, adding a DNA construct encoding Rv0919 blocked synthesis, although only when acetyl coenzyme A was added (Fig. 1D). This suggests that Rv0919 uses acetyl coenzyme A as an acetyl group donor, which has been seen with other TacAT systems (14). A construct encoding Rv0919 with an active site mutation homologous to one identified in *Salmonella* (Y138F in *M. tuberculosis*) partially abrogated protein synthesis (Fig. 1E) (13). These results suggest that Rv0919 inhibits growth by acetylating a component of the protein synthesis apparatus.

All other described TacAT-like systems encode a toxin that acetylates the amino acid on charged tRNA. Different organism toxins acetylate different tRNAs. For instance, in *Salmonella*, three different TacT-like toxins have been described. These block elongation by acetylating glycyl, isoleucyl-, leucyl-, and, to a lesser extent, other aminoacyl tRNAs *in vitro* (13) but solely glycyl-tRNA *in vivo* (in preparation). Meanwhile, in *E. coli*, the GNAT toxin AtaT was initially thought to block the initiation of protein synthesis by acetylating methionine on initiator fMet-tRNA (17) but was more recently reported to acetylate preferentially glycyl-tRNA alongside others (19). We hypothesized that *M. tuberculosis* TacT also acetylates charged tRNAs. To identify if any and which tRNA species might be affected by this enzyme, we purified total RNA from *M. smegmatis* overexpressing *M. tuberculosis* TacT and used liquid chromatography-coupled mass spectrometry (LCMS) to analyze tRNAs (Fig. 2A). A strong acetylation peak was detected for glycyl-tRNA (Fig. 2B; Table S1) but not for any other tRNAs, indicating that *M. tuberculosis* TacT specifically acetylates glycyl-tRNAs.

Peptidyl tRNA hydrolase (Pth) reverses TacT-induced translation inhibition. Previous work has shown that the enzyme peptidyl tRNA hydrolase (Pth) detoxifies the effects of TacT acetylation by cleaving acetylated amino acids from corrupted tRNAs (14). To test whether *M. tuberculosis* Pth reverses TacT activity, we purified recombinant *M. tuberculosis* Pth and added it to our cell-free protein synthesis assay (Fig. S1). Indeed, purified Pth was sufficient to rescue GFP expression in the presence of active *M. tuberculosis* TacT and acetyl coenzyme A (Fig. 3B) but had no effects on translation in the presence of catalytically inactive TacT (Fig. 3A and B). Thus, *M. tuberculosis* Pth also cleaves N-acetylated aminoacyl-tRNA thereby counteracting the effect of the toxin.

***tacAT* does not affect *pth* essentiality in *M. tuberculosis*.** In addition to reversing the effects of TacT-like toxins, Pth's primary known function is to cleave short peptides from peptidyl-tRNAs that are prematurely released from stalled ribosomes (23, 24). Similar to other bacteria, transposon sequencing (TnSeq) data suggest that *pth* is essential in *M. tuberculosis* (20). We built *M. tuberculosis pth* transcriptional knockdowns using CRISPR interference (CRISPRi) (25). Cells induced for *pth* depletion showed a marked growth defect, confirming that Pth is required for normal growth (Fig. 4).

Given TacAT's connection to this essential enzyme, we assessed whether it contributes to *pth* essentiality in *M. tuberculosis*. Transposon sequencing data indicate that the TacAT-encoding operon Rv0918-0919 is nonessential for *M. tuberculosis* growth *in vitro*, and we have identified premature stop mutations in this TA system in clinical isolates, suggesting it is also dispensable *in vivo* (Table S2) (20). We built in-frame deletions of *tacAT* in *M. tuberculosis* and used CRISPRi to knock down *pth* in this strain. In the absence of *tacAT*, *pth* knockdowns still failed to grow normally *in vitro*, suggesting that while the *tacAT* operon is dispensable, *pth* essentiality is unaffected by the absence of this TA system (Fig. 4). We also performed LCMS on *M. tuberculosis* induced or uninduced for *pth* knockdown and were unable to detect glycyl-tRNA acetylation in either strain grown (Fig. S2). Thus, growth defects of a *pth* knockdown *in vitro* are not a result of the accumulation of acetylated glycyl-tRNAs.
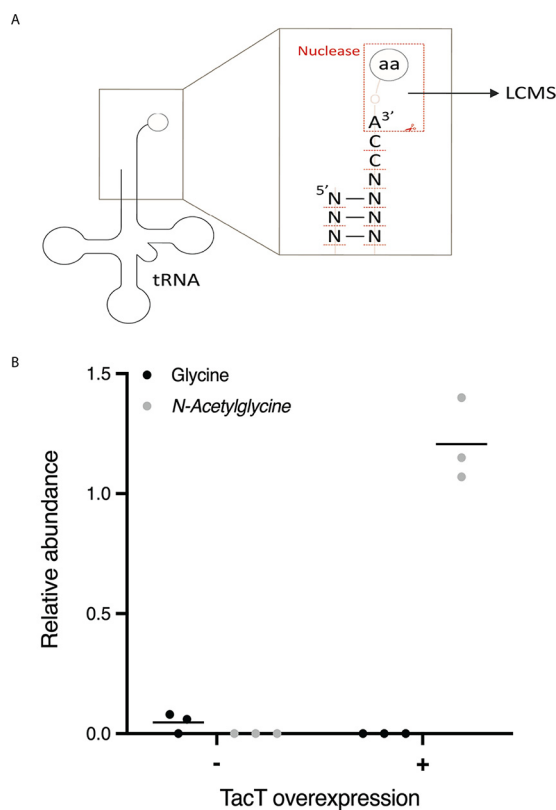
FIG 2 TacT acetylates glycyl-tRNA. *M. smegmatis* overexpressing *M. tuberculosis tacT* was grown to mid-log-phase and induced for 3 h. (A) Total RNA from triplicate cultures was collected along with an uninduced control for LCMS as described. (B) The relative abundance of unacetylated and *N*-acetylated glycyl-tRNA fragments is shown.

DISCUSSION

Toxin-antitoxin (TA) systems have been identified in most bacterial genomes and have been implicated in a variety of physiological functions ranging from phage protection and plasmid maintenance to pathogenesis and the general stress response. Interestingly, *Mycobacterium tuberculosis* encodes one of the largest repertoires of TA systems in bacteria, yet plasmids are absent from this organism (26). Furthermore, the role of TA systems in *M. tuberculosis* against bacteriophages is still under study (27). It is tempting to speculate that *M. tuberculosis*'s broad TA system toolkit serves as a growth regulator during human infection. However, experimental evidence for this is lacking, largely due to the difficulties of systematically deleting many genes simultaneously in *M. tuberculosis* and overlapping mechanisms of action that make it difficult to directly measure the activity of individual toxins. Some studies have examined the roles of individual TA systems in *M. tuberculosis* using genetic deletions and overexpression systems and linked the activity of some toxins to pathogenesis (10, 28, 29). Nonetheless, the level and spectrum of TA system involvement during *M. tuberculosis* infection remain unresolved.

Here, we have identified and characterized a TA system in *M. tuberculosis* whose mechanism of action is distinct from the other known TA systems in this organism. While most toxins in *M. tuberculosis* are ribonucleases, TacT instead blocks growth by acetylating charged tRNAs. This activity can be detected using liquid chromatography-coupled mass spectrometry (LCMS), making it an appealing TA system to study in its native form. We have shown that *M. tuberculosis* TacT acetylates glycyl tRNAs using an overexpression construct in *M. smegmatis* but have been unable to detect this modification in wild-type *M. tuberculosis*. Future work that increases the sensitivity and throughput of LCMS-based or other forms of detection for tRNA acetylation will allow researchers to probe the effects of various physiological conditions
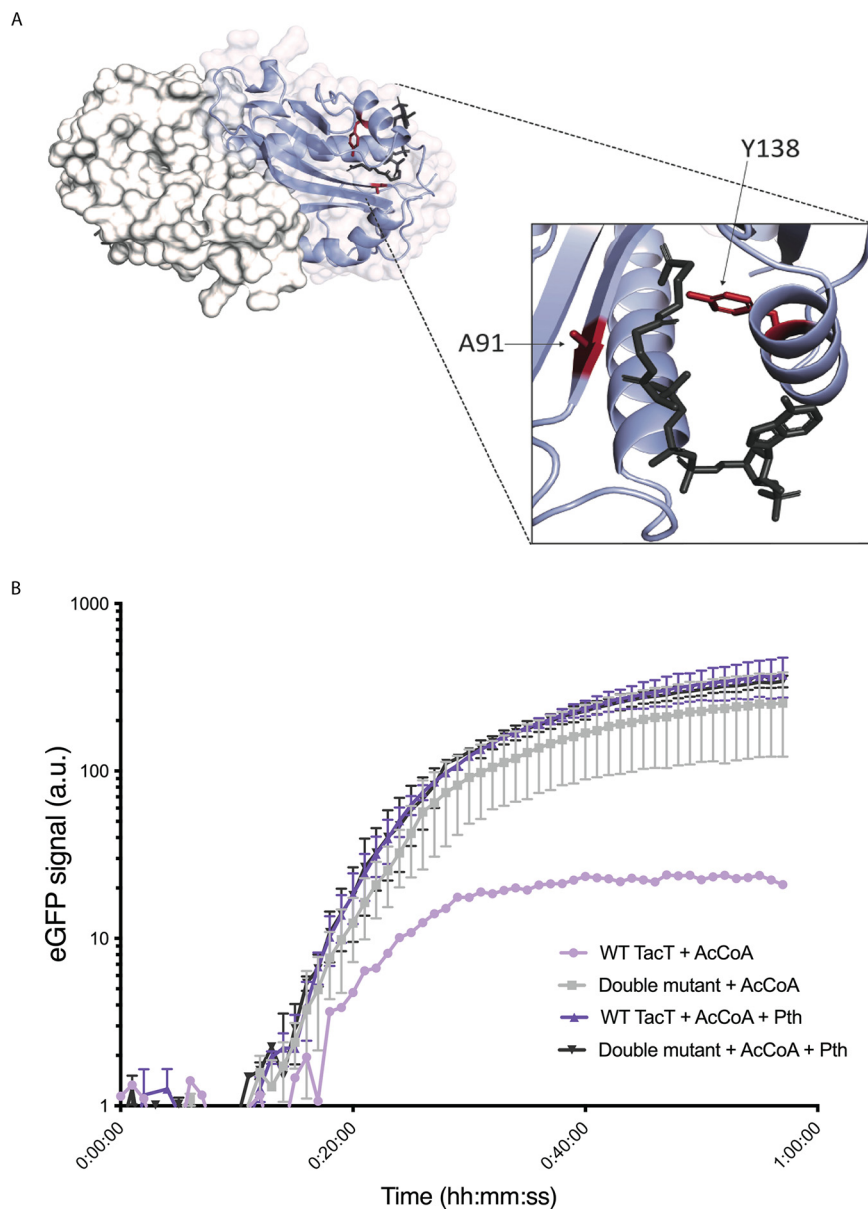
FIG 3 *M. tuberculosis* Pth detoxifies TacT. (A) Model of *M. tuberculosis* TacT dimer generated as described in Fig. 1, with one monomer showing mutations for catalytic inactivation (Y138F and A91P; red). Acetyl coenzyme A is shown in the TacT binding pocket and colored by element. (B) Cell-free protein synthesis reactions were set up as described in Fig. 1. Inactive TacT ("Double mutant") was made using an Rv0919 expression construct containing both active side residue mutations Y138F and A91P. Purified *M. tuberculosis* peptidyl tRNA hydrolase (Pth) was added where indicated (8 μM), as was acetyl coenzyme A (AcCoA; 2 nM). In reactions without Pth, an equal volume of storage buffer was added. Protein synthesis was read out as eGFP synthesis and monitored spectrophotometrically at excitation of 488 nm and emission of 509 nm. Results are from technical duplicates.

on this tRNA modification and identify conditions during which TacT is activated in *M. tuberculosis* and other bacteria containing homologous TA systems.

Recent work using genome sequences from clinical isolates of *M. tuberculosis* has shed light on the selective pressures imposed on *M. tuberculosis*'s genome during human infection (30, 31). The essentiality of a gene is correlated with its level of tolerance for nonsynonymous mutations (32). We have found that the TacAT operon in *M. tuberculosis* is dispensable *in vitro*, and clinical genomic data support that this operon is also dispensable *in vivo*, given many nonsynonymous mutations – including premature stop codons that have accumulated in clinical strains.
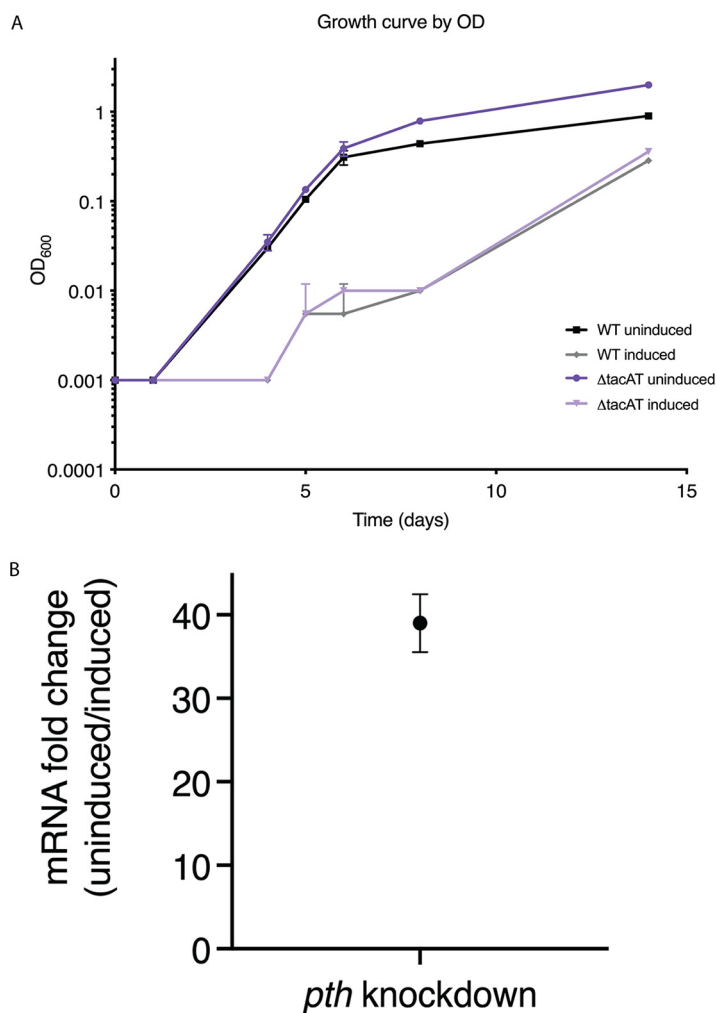
FIG 4 *pth* is required for normal growth of an *M. tuberculosis* tacAT knockout. (A) *MtbΔtacAT* and WT *M. tuberculosis* (H37Rv; parental strain) were transformed with *pth* knockdown constructs using mycobacterial CRISPR-interference (CRISPRi). Strains were diluted to an OD600 of 0.001 and either induced for *pth* knockdown (100 ng/mL aTC) or uninduced. Growth was measured by optical density at 600 nm (OD_{600}). Results are from biological duplicates. (B) Changes in *pth* transcript levels during a knockdown, as measured by RT-qPCR. Relative fold change of each mRNA was quantified by normalization to levels of *M. tuberculosis sigA* transcript. Points represent the mean of three biological replicates, with error bars depicting standard deviation.

The other unique aspect of TacAT is its mechanistic connection to the essential enzyme peptidyl tRNA hydrolase (Pth), which reverses TacT-induced aminoacyl tRNA acetylation. Pth is ubiquitous and thought to be essential across bacteria. The three critical active site residues His22, Asp95, and Asn116 are universally conserved (33). Archaea, meanwhile, encode a conserved functional homolog, *pth2*, which does not share significant sequence similarity to bacterial *pth* (33). Most eukaryotes contain both *pth* and *pth2* genes, though these enzymes are individually nonessential. Interestingly, structural studies have found that mycobacterial Pth is divergent from other bacterial Pth in several regions (34, 35). Because of its essentiality in bacteria and unique structure in mycobacteria, in addition to the vulnerability of translation rescue systems in *M. tuberculosis*, Pth has been proposed as an intriguing drug target in difficult-to-treat organisms like *M. tuberculosis* (34, 36, 37). Understanding the critical functions of Pth is important from a drug development perspective, especially when considering potential sources for antibiotic resistance. For instance, if TacT activity were a significant source for *pth* essentiality in *M. tuberculosis*, then inhibitors targeting Pth would lose efficacy in clinical isolates with a disrupted *tacAT* operon. Our work has shown that *M. tuberculosis* TacT's connection to Pth is not the source

of *pth* essentiality. This bodes well for studies of Pth as an antibiotic target because mutations inactivating *tacAT* have already been identified in clinical isolates. Finally, biochemical assays to assess Pth inhibitors can exploit the relationship between Pth and TacT using *in vitro* protein synthesis kits by screening for loss of Pth-mediated detoxification.

MATERIALS AND METHODS

Bacterial strains and growth conditions. *M. tuberculosis* and *M. smegmatis* strains were grown from frozen stocks into Middlebrook 7H9 medium supplemented with 0.2% glycerol, 0.05% Tween 80, and ADC (5g/L bovine serum albumin, 2g/L dextrose, 3 μg/mL catalase). Cultures were incubated at 37°C. Antibiotics or inducing agents were used when needed at the following concentrations in both *M. tuberculosis* and *M. smegmatis*: kanamycin (25 μg/mL), anhydrous tetracycline (aTC; 100 ng/mL), hygromycin (50 μg/mL), and nourseothricin (20 μg/mL). Transformed *M. tuberculosis* and *M. smegmatis* strains were plated onto 7H10 agar plates with the appropriate antibiotic(s). Strains were grown to mid-log-phase for all experiments unless otherwise specified (optical density at 600 nm (OD_{600}) 0.4 to 0.6). *E. coli* strains for cloning or protein purification were grown in LB broth or on LB agar with appropriate antibiotics at the following concentrations: kanamycin (50 μg/mL), zeocin (50 μg/mL), and nourseothricin (40 μg/mL). The induction time for *pth* depletion in *M. tuberculosis* was 4 days. Induction for *tacT* overexpression in *M. smegmatis* was 3 h.

Bacterial strain construction. Table S3 depicts the strains, plasmids, primers, and recombinant DNA used for this study. Plasmids were built by restriction digest of a parental vector and inserts were prepared either by restriction enzyme cloning or Gibson assembly (38) using 40 bp overhangs, as specified in Table S3. Plasmids were isolated from *E. coli* and confirmed via Sanger sequencing carried out by Genewiz, LLC (MA, USA).

Deletion mutants. The knockout strain Δ*tacAT*::zeo (zeocin) was built using double-stranded recombineering in the parental *M. tuberculosis* strain H37Rv. A linear dsDNA fragment was constructed using stitch PCR with the primers listed in Table S3, which consisted of a 500 bp region upstream of the *tacAT* operon (Rv0918-019), 500 bp downstream region, and a *lox*-zeo-*lox* fragment. This cassette was transformed into an H37Rv recombineering strain as described (39) and plated on 7H10 + zeocin plates.

tacAT and tacT alleles. Plasmid FT2, used for inducible *tact* overexpression in *M. smegmatis*, was generated using a parental vector (CT16) that integrates into the L5 mycobacterial phage site. This plasmid also encodes kanamycin resistance and contains both the tet promoter (directly upstream of *tacT*) and the tet repressor. CT16 was digested with ClaI and XbaI (New England Biolabs). *tacT* (Rv0919) was PCR-amplified and ligated into the plasmid using restriction cloning. Plasmid FT3, used for *tacAT* overexpression, was generated by placing *tacAT* together under the constitutive UV15 promoter in a parental vector (CT250) which was digested with NdeI and HindIII (New England Biolabs). The *tacAT* operon Rv0918-0919 was ligated to the plasmid using Gibson cloning.

Pth-knockdown constructs. Transcriptional knockdown of *pth* was accomplished using mycobacterial CRISPRi-interference (CRISPRi). Knockdown constructs were built as previously described (25) by annealing oligonucleotides for *pth* and ligating them into a linearized BsmBI-digested plasmid (CT 296; a gift from Jeremy Rock) that contains mycobacterial CRISPRi. The knockdown vector FT110 was transformed in both H37Rv wild type (WT) and Δ*tacAT*::ZeoR.

Purification of M. tuberculosis Pth. *M. tuberculosis pth* (Rv1014c) was cloned with a C-terminal 6× His tag and expressed from pET28a in BL21-CodonPlus (DE3)-RP *E. coli* under conditions similar to those previously described (40). One liter of log-phase culture (OD_{600} ~0.7) was induced with 1 mM isopropyl β-D-1-thiogalactopyranoside (IPTG) for 4 h at 37°C. Cells were harvested at 6,000g for 15 min, and the resulting pellet was frozen at −80°C. The pellet was thawed with a stir-bar at 4°C in lysis buffer containing 50 mM Tris HCl pH 7.5, 300 mM NaCl, 10% glycerol, DNase powder, 1 tablet complete EDTA-free protease inhibitor, and 2 mM 2-mercaptoethanol (BME), and cells were lysed using a French press. The lysate was clarified by spinning at 30,000g for 30 min and brought up to 20 mM imidazole pH 7.5. His-tagged Pth was then extracted via batch binding 2.5 mL equilibrated Ni-NTA beads incubated with lysate for 1 h at 4°C. Beads were collected and washed with 20 mL lysis buffer containing 2 mM BME. A second wash included 20 mL lysis buffer with 20 mM imidazole and 2 mM BME, followed by 5 mL of lysis buffer with 30 mM imidazole, and a final wash with 5 mL lysis buffer containing 40 mM imidazole and 2 mM BME. Samples were eluted with lysis buffer containing 200 mM imidazole pH 7.5 in 750 μL fractions and analyzed via SDS-PAGE (Fig. S1, left). The cleanest elution fractions (4 to 6 and 7 to 9) were desalted into lysis buffer containing BME, concentrated with a 10 kDa MWCO amicon ultra 4 spin column to 1 mL, and further purified by FPLC via gel filtration chromatography with a Superdex 75 Increase 10/300 GL column in buffer containing (25 mM Tris-HCl pH 7.5, 150 mM NaCl, 2 mM BME). Fractions were analyzed via SDS-PAGE (Fig. S1, right) and fractions 2d2-2d3 (at an elution volume of ~13 mL) were pooled and brought up to 5% glycerol with 2 mM fresh BME. Nanodrop readings suggested that other fractions containing what appeared to be pure Pth were contaminated by unknown nucleic acid species. Nucleic acid-free protein (fractions 2d2-2d3) was aliquoted into 10 μL aliquots, flash-frozen with liquid nitrogen, and stored at −80°C. Pth protein concentration was calculated using a Coomassie Plus (Bradford) Assay (Pierce).

In vitro translation. To assess the effect of TacT on translation, *in vitro* translation reactions were prepared with purified *tacT* DNA (WT, Y138F, or Y138F/A91P), 2 nM acetyl coenzyme A, and purified Pth. A master mix of purified eGFP DNA (200 ng per reaction), *tact* DNA (180 ng per reaction), and PURExpress (New England Biolabs) components were prepared in triplicate reactions with 8 μM Pth and 2 nM acetyl

coenzyme A. When no Pth was added, an equal volume of storage buffer was used in place of protein. When no acetyl coenzyme A was added, an equal volume of water was added. Reactions were carried out in 12 μL in a black Costar 384-well plate for 2 h at 37°C, and eGFP fluorescence (excitation = 488 nm and emission = 509 nm) was measured over time on a SpectraMax M2 microplate reader.

mRNA quantification. Ten milliliters of *M. tuberculosis* cultures were harvested at 4,000 rpm for 10 min and pellets were resuspended in 1 mL TRIzol reagent (ThermoFisher Scientific). Samples were lysed by bead beating. Purified DNase-treated RNA was used as the template for cDNA synthesis, following the manufacturer's instructions with Superscript IV (Life Technologies). RNA was removed using RNase A (ThermoFisher Scientific) and cDNA was cleaned up by column purification (Zymo Research). qPCR was performed using iTaq Universal SYBR Green Supermix (Bio-Rad). mRNA fold change was calculated using the $\Delta\Delta$Ct method, where *pth* transcript level was normalized by *sigA* level under each condition.

Liquid chromatography-coupled mass spectrometry. Purified RNA (30 to 50 μg) was spiked with 1 μM ^{15}N-AMP and incubated with 1U Nuclease P1 in 10 mM ammonium acetate for 30 min at 25°C (Fig. 2 and Fig. S2). Alternatively, purified RNA was incubated with 25 μg purified Pth in buffer (10 mM Tris-acetate, 10 mM magnesium acetate, 20 mM ammonium acetate pH 8) for 1 h at 37°C. Processed RNA samples were diluted 1:3 with acetonitrile + 0.2% vol/vol acetic acid, centrifuged for 10 min at 21,000 $\times$ *g*, room temperature to remove any precipitate, and transferred to glass microvials. Samples were analyzed on a Thermo Ultimate 3000 LC coupled with a Q-Exactive Plus mass spectrometer in both positive and negative ion modes. Five microliters of each sample were injected on a Zic-pHILIC Column (150 $\times$ 2.1 mm, 5 μm particles, EMD Millipore). The mobile phases are (A) 20 mM ammonium carbonate in 0.1% ammonium hydroxide and (B) acetonitrile 97% in water. The gradient conditions were as follows: 100% B at 0 min, 40% B at 20 min, 0% B at 30 min for 5 min, then back to 100% B in 5 min, followed by 10 min of re-equilibration. A constant flow rate of 0.200 L/minute was used. The mass spectrometer was calibrated immediately before use. Data were analyzed using Thermo Xcalibur 3.0 with ICIS automated peak integration (Default settings: Smoothing Points = 9; Baseline Window = 40; Area Noise Factor = 2; Peak Noise Factor = 10) followed by manual data curation. In the analysis of NP1 treated samples (Fig. 2 and Fig. S2), peak areas were normalized relative to the peak area of the ^{15}N-AMP spike-in. To distinguish between isobaric tRNA fragments derived from *N*-acetylserine and glutamic acid ([M+H]+ ion *m/z* = 476.1057), RNA samples instead treated with Pth (to cleave *N*-acetyl amino acids from tRNAs) were compared by LC/MS to purified standards of each amino acid, allowing for identification of peaks discriminated by retention time (Fig. S3). These data indicate that glutamic acid, and not *N*-acetylserine, contributes the entirety of the MS signal detected for ions with an *m/z* of 147.0532 and that TacT does not acetylate seryl-tRNA.

Whole-genome sequencing analysis of clinical isolates. Whole-genome sequences of 55778 *M. tuberculosis* isolates were obtained from 211 BioProjects under the following accession codes: ERP001037, ERP002611, ERP008770, PRJDB10607, PRJDB3875, PRJDB6149, PRJDB7006, PRJDB8544, PRJDB8553, PRJEB10385, PRJEB10533, PRJEB10577, PRJEB10950, PRJEB11460, PRJEB11653, PRJEB11778, PRJEB12011, PRJEB12179, PRJEB12184, PRJEB12764, PRJEB13325, PRJEB13764, PRJEB13960, PRJEB14199, PRJEB15076, PRJEB15382, PRJEB15857, PRJEB18529, PRJEB20214, PRJEB21888, PRJEB21922, PRJEB23245, PRJEB23495, PRJEB2358, PRJEB23648, PRJEB23664, PRJEB23996, PRJEB24463, PRJEB25506, PRJEB25543, PRJEB25592, PRJEB25814, PRJEB25968, PRJEB25971, PRJEB25972, PRJEB25991, PRJEB25997, PRJEB25998, PRJEB25999, PRJEB26000, PRJEB26001, PRJEB26002, PRJEB27244, PRJEB27354, PRJEB27366, PRJEB27446, PRJEB27847, PRJEB2794, PRJEB28497, PRJEB28842, PRJEB29199, PRJEB29276, PRJEB29408, PRJEB29435, PRJEB29446, PRJEB29604, PRJEB30463, PRJEB30782, PRJEB30933, PRJEB31023, PRJEB31905, PRJEB32037, PRJEB32234, PRJEB32341, PRJEB32589, PRJEB32684, PRJEB32773, PRJEB33896, PRJEB35201, PRJEB39699, PRJEB40777, PRJEB5162, PRJEB5280, PRJEB5899, PRJEB5925, PRJEB6273, PRJEB6717, PRJEB6945, PRJEB7056, PRJEB7281, PRJEB7669, PRJEB7727, PRJEB7798, PRJEB8311, PRJEB8432, PRJEB8689, PRJEB9003, PRJEB9201, PRJEB9206, PRJEB9308, PRJEB9545, PRJEB9680, PRJEB9709, PRJEB9976, PRJNA200335, PRJNA217391, PRJNA219826, PRJNA220218, PRJNA229360, PRJNA233386, PRJNA235852, PRJNA237443, PRJNA244659, PRJNA254678, PRJNA259657, PRJNA268900, PRJNA270137, PRJNA282721, PRJNA287858, PRJNA295328, PRJNA300846, PRJNA302362, PRJNA305488, PRJNA306588, PRJNA308536, PRJNA318002, PRJNA352769, PRJNA353873, PRJNA354716, PRJNA355614, PRJNA356104, PRJNA361483, PRJNA369219, PRJNA376471, PRJNA377769, PRJNA379070, PRJNA384604, PRJNA384765, PRJNA384815, PRJNA385247, PRJNA388806, PRJNA390065, PRJNA390291, PRJNA390471, PRJNA393378, PRJNA393923, PRJNA393924, PRJNA401368, PRJNA401515, PRJNA407704, PRJNA413593, PRJNA414758, PRJNA419964, PRJNA421323, PRJNA421446, PRJNA428596, PRJNA429460, PRJNA430531, PRJNA431049, PRJNA436223, PRJNA436997, PRJNA438921, PRJNA448595, PRJNA453687, PRJNA454477, PRJNA475130, PRJNA475771, PRJNA480117, PRJNA480888, PRJNA481625, PRJNA481638, PRJNA482095, PRJNA482716, PRJNA482865, PRJNA486713, PRJNA488343, PRJNA488426, PRJNA492975, PRJNA506272, PRJNA509547, PRJNA512266, PRJNA522942, PRJNA523164, PRJNA523499, PRJNA524863, PRJNA526078, PRJNA533314, PRJNA540911, PRJNA549270, PRJNA559678, PRJNA566379, PRJNA573497, PRJNA578162, PRJNA586859, PRJNA587747, PRJNA589048, PRJNA591498, PRJNA595834, PRJNA598949, PRJNA598981, PRJNA608715, PRJNA632617, PRJNA663350, PRJNA678116, PRJNA679443, PRJNA683067, PRJNA684613, PRJNA688213, SRP018402. The Sickle tool was used for trimming whole-genome sequencing data (41). Sequencing reads with Phred base quality scores above 20 and read lengths longer than 30 were kept for analysis. The inferred ancestral genome of the most recent common ancestor of the MTBC was used as the reference template for read mapping (42). Sequencing reads were mapped to the reference genome using Bowtie 2 (version 2.2.9) (43). SAMtools (v1.3.1) was used for SNP calling with mapping quality greater than 30. Fixed mutations (frequency $\geq$ 75%) were identified using VarScan (v2.3.9) with at least 10 supporting reads and the strand bias filter option on. SNPs in repetitive regions of

the genome (e.g., PPE/PE-PGRS family genes, phage sequences, insertion, or mobile genetic elements) were excluded (44, 45).

Data availability. The data that support these findings are available from the corresponding author upon reasonable request.

SUPPLEMENTAL MATERIAL

Supplemental material is available online only.

SUPPLEMENTAL FILE 1, XLSX file, 0.05 MB.
SUPPLEMENTAL FILE 2, XLSX file, 0.01 MB.
SUPPLEMENTAL FILE 3, XLSX file, 0.01 MB.
SUPPLEMENTAL FILE 4, PDF file, 0.1 MB.

REFERENCES

1. World Health Organization. 2021. Global tuberculosis report 2021.
2. Fernandez-Garcia L, Blasco L, Lopez M, Bou G, García-Contreras R, Wood T, Tomas M. 2016. Toxin-antitoxin systems in clinical pathogens. Toxins (Basel) 8:227. https://doi.org/10.3390/toxins8070227.
3. Gupta A, Venkataraman B, Vasudevan M, Gopinath Bankar K. 2017. Co-expression network analysis of toxin-antitoxin loci in Mycobacterium tuberculosis reveals key modulators of cellular stress. Sci Rep 7:5868. https://doi.org/10.1038/s41598-017-06003-7.
4. Slayden RA, Dawson CC, Cummings JE. 2018. Toxin-antitoxin systems and regulatory mechanisms in Mycobacterium tuberculosis. Pathog Dis 76. https://doi.org/10.1093/femspd/fty039.
5. Sala A, Bordes P, Genevaux P. 2014. Multiple toxin-antitoxin systems in Mycobacterium tuberculosis. Toxins (Basel) 6:1002–1020. https://doi.org/10.3390/toxins6031002.
6. Fraikin N, Goormaghtigh F, Van Melderen L. 2020. Type II toxin-antitoxin systems: evolution and revolutions. J Bacteriol 202:e00763-19. https://doi.org/10.1128/JB.00763-19.
7. Helaine S, Kugelberg E. 2014. *B*acterial persisters: formation, eradication, and experimental systems. Trends Microbiol 22:417–424. https://doi.org/10.1016/j.tim.2014.03.008.
8. Page R, Peti W. 2016. Toxin-antitoxin systems in bacterial growth arrest and persistence. Nat Chem Biol 12:208–214. https://doi.org/10.1038/nchembio.2044.
9. Ramage HR, Connolly LE, Cox JS. 2009. Comprehensive functional analysis of Mycobacterium tuberculosis toxin-antitoxin systems: implications for pathogenesis, stress responses, and evolution. PLoS Genet 5:e1000767. https://doi.org/10.1371/journal.pgen.1000767.
10. Tiwari P, Arora G, Singh M, Kidwai S, Narayan OP, Singh R. 2015. MazF ribonucleases promote Mycobacterium tuberculosis drug tolerance and virulence in guinea pigs. Nat Commun 6:6059. https://doi.org/10.1038/ncomms7059.
11. LeRoux M, Culviner PH, Liu YJ, Littlehale ML, Laub MT. 2020. Stress can induce transcription of toxin-antitoxin systems without activating toxin. Mol Cell 79:280–292.e8. https://doi.org/10.1016/j.molcel.2020.05.028.
12. Ramirez MV, Dawson CC, Crew R, England K, Slayden RA. 2013. MazF6 toxin of Mycobacterium tuberculosis demonstrates antitoxin specificity

and is coupled to regulation of cell growth by a Soj-like protein. BMC Microbiol 13:240. https://doi.org/10.1186/1471-2180-13-240.
13. Rycroft JA, Gollan B, Grabe GJ, Hall A, Cheverton AM, Larrouy-Maumus G, Hare SA, Helaine S. 2018. Activity of acetyltransferase toxins involved in Salmonella persister formation during macrophage infection. Nat Commun 9:1993. https://doi.org/10.1038/s41467-018-04472-6.
14. Cheverton AM, Gollan B, Przydacz M, Wong CT, Mylona A, Hare SA, Helaine S. 2016. A Salmonella toxin promotes persister formation through acetylation of tRNA. Mol Cell 63:86–96. https://doi.org/10.1016/j.molcel.2016.05.002.
15. Wilcox B, Osterman I, Serebryakova M, Lukyanov D, Komarova E, Gollan B, Morozova N, Wolf YI, Makarova KS, Helaine S, Sergiev P, Dubiley S, Borukhov S, Severinov K. 2018. *Escherichia coli* ItaT is a type II toxin that inhibits translation by acetylating isoleucyl-tRNAIle. Nucleic Acids Res 46:7873–7885. https://doi.org/10.1093/nar/gky560.
16. Qian H, Yao Q, Tai C, Deng Z, Gan J, Ou H-Y. 2018. Identification and characterization of acetyltransferase-type toxin-antitoxin locus in *Klebsiella pneumoniae*. Mol Microbiol 108:336–349. https://doi.org/10.1111/mmi.13934.
17. Jurenas D, Chatterjee S, Konijnenberg A, Sobott F, Droogmans L, Garcia-Pino A, Van Melderen L. 2017. AtaT blocks translation initiation by N-acetylation of the initiator tRNA(fMet). Nat Chem Biol 13:640–646. https://doi.org/10.1038/nchembio.2346.
18. Zhang C, Yashiro Y, Sakaguchi Y, Suzuki T, Tomita K. 2020. Substrate specificities of Escherichia coli ItaT that acetylates aminoacyl-tRNAs. Nucleic Acids Res 48:7532–7544.
19. Yashiro Y, Sakaguchi Y, Suzuki T, Tomita K. 2020. Mechanism of aminoacyl-tRNA acetylation by an aminoacyl-tRNA acetyltransferase AtaT from enterohemorrhagic *E. coli*. Nat Commun 11:5438. https://doi.org/10.1038/s41467-020-19281-z.
20. DeJesus MA, Gerrick ER, Xu W, Park SW, Long JE, Boutte CC, Rubin EJ, Schnappinger D, Ehrt S, Fortune SM, Sassetti CM, Ioerger TR. 2017. Comprehensive essentiality analysis of the Mycobacterium tuberculosis genome via saturating transposon mutagenesis. mBio 8:e02133-16. https://doi.org/10.1128/mBio.02133-16.

21. Kapopoulou A, Lew JM, Cole ST. 2011. The MycoBrowser portal: a comprehensive and manually annotated resource for mycobacterial genomes. Tuberculosis (Edinb) 91:8–13. https://doi.org/10.1016/j.tube.2010.09.006.

22. Altschul SF, Gish W, Miller W, Myers EW, Lipman DJ. 1990. Basic local alignment search tool. J Mol Biol 215:403–410. https://doi.org/10.1016/S0022-2836(05)80360-2.

23. Das G, Varshney U. 2006. Peptidyl-tRNA hydrolase and its critical role in protein biosynthesis. Microbiology (Reading) 152:2191–2195. https://doi.org/10.1099/mic.0.29024-0.

24. Sharma S, Kaushik S, Sinha M, Kushwaha GS, Singh A, Sikarwar J, Chaudhary A, Gupta A, Kaur P, Singh TP. 2014. Structural and functional insights into peptidyl-tRNA hydrolase. Biochim Biophys Acta 1844:1279–1288. https://doi.org/10.1016/j.bbapap.2014.04.012.

25. Rock JM, Hopkins FF, Chavez A, Diallo M, Chase MR, Gerrick ER, Pritchard JR, Church GM, Rubin EJ, Sassetti CM, Schnappinger D, Fortune SM. 2017. Programmable transcriptional repression in mycobacteria using an orthogonal *CRISPR* interference platform. Nat Microbiol 2:16274. https://doi.org/10.1038/nmicrobiol.2016.274.

26. Zainuddin ZF, Dale JW. 1990. Does Mycobacterium tuberculosis have plasmids? Tubercle 71:43–49. https://doi.org/10.1016/0041-3879(90)90060-L.

27. Lobato-Marquez D, Diaz-Orejas R, Garcia del Portillo F. 2016. Toxin-antitoxins and bacterial virulence. FEMS Microbiol Rev 40:592–609. https://doi.org/10.1093/femsre/fuw022.

28. Sharma A, Chattopadhyay G, Chopra P, Bhasin M, Thakur C, Agarwal S, Ahmed S, Chandra N, Varadarajan R, Singh R. 2020. VapC21 toxin contributes to drug-tolerance and interacts with non-cognate VapB32 antitoxin in Mycobacterium tuberculosis. Front Microbiol 11:2037. https://doi.org/10.3389/fmicb.2020.02037.

29. Talwar S, Pandey M, Sharma C, Kutum R, Lum J, Carbajo D, Goel R, Poidinger M, Dash D, Singhal A, Pandey AK. 2020. Role of VapBC12 toxin-antitoxin locus in cholesterol-induced Mycobacterial persistence. mSystems 5:e00855-20. https://doi.org/10.1128/mSystems.00855-20.

30. Meehan CJ, Goig GA, Kohl TA, Verboven L, Dippenaar A, Ezewudo M, Farhat MR, Guthrie JL, Laukens K, Miotto P, Ofori-Anyinam B, Dreyer V, Supply P, Suresh A, Utpatel C, van Soolingen D, Zhou Y, Ashton PM, Brites D, Cabibbe AM, de Jong BC, de Vos M, Menardo F, Gagneux S, Gao Q, Heupink TH, Liu Q, Loiseau C, Rigouts L, Rodwell TC, Tagliani E, Walker TM, Warren RM, Zhao Y, Zignol M, Schito M, Gardy J, Cirillo DM, Niemann S, Comas I, Van Rie A. 2019. Whole genome sequencing of Mycobacterium tuberculosis: current standards and open issues. Nat Rev Microbiol 17:533–545. https://doi.org/10.1038/s41579-019-0214-5.

31. Stucki D, Brites D, Jeljeli L, Coscolla M, Liu Q, Trauner A, Fenner L, Rutaihwa L, Borrell S, Luo T, Gao Q, Kato-Maeda M, Ballif M, Egger M, Macedo R, Mardassi H, Moreno M, Tudo Vilanova G, Fyfe J, Globan M, Thomas J, Jamieson F, Guthrie JL, Asante-Poku A, Yeboah-Manu D, Wampande E, Ssengooba W, Joloba M, Henry Boom W, Basu I, Bower J, Saraiva M, Vaconcellos SEG, Suffys P, Koch A, Wilkinson R, Gail-Bekker L, Malla B, Ley SD, Beck H-P, de Jong BC, Toit K, Sanchez-Padilla E, Bonnet M, Gil-Brusola A, Frank M, Penlap Beng VN, Eisenach K, Alani I, Wangui Ndung'u P. 2016. *Mycobacterium tuberculosis* lineage 4 comprises globally distributed and geographically restricted sublineages. Nat Genet 48:1535–1543. https://doi.org/10.1038/ng.3704.

32. Liu Q, Wei J, Li Y, Wang M, Su J, Lu Y, López MG, Qian X, Zhu Z, Wang H, Gan M, Jiang Q, Fu Y-X, Takiff HE, Comas I, Li F, Lu X, Fortune SM, Gao Q. 2020. *Mycobacterium tuberculosis* clinical isolates carry mutational signatures of host immune environments. Sci Adv 6:eaba4901. https://doi.org/10.1126/sciadv.aba4901.

33. Rosas-Sandoval G, Ambrogelly A, Rinehart J, Wei D, Cruz-Vera LR, Graham DE, Stetter KO, Guarneros G, Söll D. 2002. Orthologs of a novel archaeal and of the bacterial peptidyl-tRNA hydrolase are nonessential in yeast. Proc Natl Acad Sci U S A 99:16707–16712. https://doi.org/10.1073/pnas.222659199.

34. Kabra A, Fatma F, Shahid S, Pathak PP, Yadav R, Pulavarti SVSRK, Tripathi S, Jain A, Arora A. 2016. Structural characterization of peptidyl-tRNA hydrolase from Mycobacterium smegmatis by NMR spectroscopy. Biochim Biophys Acta 1864:1304–1314. https://doi.org/10.1016/j.bbapap.2016.06.013.

35. Selvaraj M, Ahmad R, Varshney U, Vijayan M. 2012. Structures of new crystal forms of Mycobacterium tuberculosis peptidyl-tRNA hydrolase and functionally important plasticity of the molecule. Acta Crystallogr Sect F Struct Biol Cryst Commun 68:124–128. https://doi.org/10.1107/S1744309111052341.

36. Alumasa JN, Manzanillo PS, Peterson ND, Lundrigan T, Baughn AD, Cox JS, Keiler KC. 2017. Ribosome rescue inhibitors kill actively growing and nonreplicating persister Mycobacterium tuberculosis cells. ACS Infect Dis 3:634–644. https://doi.org/10.1021/acsinfecdis.7b00028.

37. Keiler KC. 2015. Mechanisms of ribosome rescue in bacteria. Nat Rev Microbiol 13:285–297. https://doi.org/10.1038/nrmicro3438.

38. Gibson DG, Young L, Chuang R-Y, Venter JC, Hutchison CA, Smith HO. 2009. Enzymatic assembly of DNA molecules up to several hundred kilobases. Nat Methods 6:343–345. https://doi.org/10.1038/nmeth.1318.

39. Murphy KC, Papavinasasundaram K, Sassetti CM. 2015. Mycobacterial recombineering. Methods Mol Biol 1285:177–199. https://doi.org/10.1007/978-1-4939-2450-9_10.

40. Bal NC, Agrawal H, Meher AK, Arora A. 2007. Characterization of peptidyl-tRNA hydrolase encoded by open reading frame Rv1014c of Mycobacterium tuberculosis H37Rv. Biol Chem 388:467–479.

41. Joshi NA, Fass JN. 2011. A sliding-window, adaptive, quality-based trimming tool for FastQ files. [Software]. Available from: https://github.com/najoshi/sickle.

42. Comas I, Coscolla M, Luo T, Borrell S, Holt KE, Kato-Maeda M, Parkhill J, Malla B, Berg S, Thwaites G, Yeboah-Manu D, Bothamley G, Mei J, Wei L, Bentley S, Harris SR, Niemann S, Diel R, Aseffa A, Gao Q, Young D, Gagneux S. 2013. Out-of-Africa migration and Neolithic coexpansion of Mycobacterium tuberculosis with modern humans. Nat Genet 45:1176–1182. https://doi.org/10.1038/ng.2744.

43. Langmead B, Salzberg SL. 2012. Fast gapped-read alignment with Bowtie 2. Nat Methods 9:357–359. https://doi.org/10.1038/nmeth.1923.

44. Koboldt DC, Zhang Q, Larson DE, Shen D, McLellan MD, Lin L, Miller CA, Mardis ER, Ding L, Wilson RK. 2012. VarScan 2: somatic mutation and copy number alteration discovery in cancer by exome sequencing. Genome Res 22:568–576. https://doi.org/10.1101/gr.129684.111.

45. Li H, Handsaker B, Wysoker A, Fennell T, Ruan J, Homer N, Marth G, Abecasis G, Durbin R, 1000 Genome Project Data Processing Subgroup. 2009. The sequence alignment/map format and SAMtools. Bioinformatics 25:2078–2079. https://doi.org/10.1093/bioinformatics/btp352.

46. Kelley LA, Mezulis S, Yates CM, Wass MN, Sternberg MJE. 2015. The Phyre2 web portal for protein modeling, prediction and analysis. Nat Protoc 10:845–858. https://doi.org/10.1038/nprot.2015.053.